Available online at www.sciencedirect.com
ScienceDirect
J. Chem. Thermodynamics 38 (2006) 1260–1268
JCT
www.elsevier.com/locate/jct

# Calorimetric analysis of NaF and $NaLaF_4$

J.P.M. van der Meer [a], R.J.M. Konings [a,*], D. Sedmidubský [b], A.C.G. van Genderen [c], H.A.J. Oonk [c]

[a] European Commission, Joint Research Centre, Institute for Transuranium Elements, P.O. Box 2340, D-76125 Karlsruhe, Germany
[b] Institute of Chemical Technology, Technická 5, 16628 Prague, Czech Republic
[c] Chemical Thermodynamics Group, Utrecht University, Padualaan 8, 3584 CH Utrecht, Netherlands

Received 12 December 2005; received in revised form 6 March 2006; accepted 7 March 2006
Available online 14 March 2006

**Abstract**

Heat flux calorimetry was used to measure the heat capacity of NaF between 630 K and 1100 K. The results agreed well with previous measurements known from the literature. Similar experiments were performed on $NaLaF_4$. This compound was synthesized from NaF and $LaF_3$ and analyzed by X-ray diffraction. The heat capacity of $NaLaF_4$ was determined for two temperature ranges: from 4 K to 400 K, for which adiabatic calorimetry, and from 623 K to 1213 K for which differential scanning heat flux calorimetry was used. The two heat capacity series fit smoothly; the resulting $C_{p,m}$ function was used in a reassessment of the binary system ($NaF + LaF_3$).


*Keywords:* Heat flux calorimetry; Adiabatic calorimetry; Fluoride salts

## 1. Introduction

The compound $NaLaF_4$ was studied in the framework of our ongoing study on the thermodynamic modelling and analysis of fluoride salts, which are of interest for one of the reactor systems proposed by the Generation IV initiative. Generation IV comprises six nuclear reactor concepts for clean and safe energy for the future. One of these is the Molten Salt Reactor, which uses molten fluorides as a coolant and also as a fuel. The latter consists of a fissile material, such as $^{233}U$, $^{235}U$ and $^{239}Pu$ or other higher actinides, dissolved as a fluoride salt in a matrix of metal fluorides that have the appropriate chemical and neutronic properties. When designed for an actinide burner, a potential solvent is a eutectic melt of LiF and NaF.

As an inactive analogue for the fuel candidate ($LiF + NaF + PuF_3$), the salt composition ($LiF + NaF + LaF_3$) has been used to perform thermal and calorimetric experiments. One binary intermediate compound exists in this system, $NaLaF_4$, for which, to our best knowledge, no calorimetric data are known. It was analyzed by heat flux calorimetry to obtain heat capacity data in the temperature range from 623 K to 1213 K at the Institute for Transuranium Elements and by adiabatic calorimetry to complete the heat capacity series in the lower temperature range from 4 K to 400 K at Utrecht University.

## 2. Experimental

### 2.1. Synthesis

As fluoride salts are hygroscopic, sample preparation and measurements were carried out in an inert argon atmosphere. NaF 99.99% (on metals basis) and $LaF_3$ 99.99% (REO) from Alfa Aesar were used. The two salts were purified before use. A few grams of powdered salt in an open nickel container were heated under vacuum in a Monel tube furnace to 423 K and kept at this temperature for 12 h. Immediately after, the salts were transported to a glovebox, which was filled with dry and pure argon (grade 5.0) gas.

* Corresponding author. Tel.: +49 72 47 951 391; fax: +49 72 47 951 566.
*E-mail address:* Rudy.KONINGS@cec.eu.int (R.J.M. Konings).

0021-9614/$ - see front matter © 2006 Elsevier Ltd. All rights reserved.
doi:10.1016/j.jct.2006.03.002

In here, amounts of NaF and $LaF_3$ were carefully weighed and mixed. The synthesis was performed *in situ* in a Setaram Multi-HTC heat flux calorimeter. Platinum crucibles with a cover and with a boron nitride liner were filled with the salt mixture. The compound $NaLaF_4$ melts peritectically around 1060 K [1,2]. To reach an optimum mixing, the salt samples were heated above the melting temperature, up to 1100 K at a rate of $5\ K \cdot min^{-1}$. Then they were slowly cooled at a rate of $2\ K \cdot min^{-1}$ down to 1043 K and the samples were kept for 24 h at that temperature. After a rapid cooling to room temperature, the samples were immediately transported to the argon glovebox.

### 2.2. X-ray diffraction

X-ray diffraction analysis was performed on a sample of powdered $NaLaF_4$. In the past, Zachariasen [3] and Burns [4] made a XRD analysis on this compound and they found a trigonal and a hexagonal phase, respectively. It should be noted that, despite the fact that different crystal structures were reported, their results do not differ much. The former found a space group of P321, with cell parameters $a = b = 617.47$ pm, $c = 382.62$ pm, while the latter reported $P\bar{6}$ as space group with parameters $a = b = 615.7$ pm, $c = 382.2$ pm, which suggests that the hexagonal cell can be superposed to the trigonal cell. Our results, for which the cell parameters $a = b = 617.471 \pm 0.072$ pm, $c = 382.62 \pm 0.058$ pm were found, are in agreement with the findings from Zachariasen. A tiny peak at $2\Theta = 36°$ could not be ascribed to the presence of $LaF_3$, NaF, LaOF or any $La(OH)_n$ compound and could not be identified.

### 2.3. Low temperature heat capacity

The low temperature heat capacity was measured by using the adiabatic calorimeter CAL V, which was developed at the Chemical Thermodynamics Group of Utrecht University [5]. The accuracy of the machine was checked for the 10 K to 100 K range using *n*-heptane and from 100 K to 400 K with sapphire (NBS Standard Reference Material 720). The differences between the measured values and the literature data were smaller than 0.1%. In a glovebox operating under a dry nitrogen atmosphere, the sample (4.31 g) was loaded in a gold container and carefully placed in the calorimeter. The sample was cooled and analyzed in two stages, first to liquid $N_2$ temperature and subsequently to the temperature of liquid He. Seven measurement series were performed of which an overview is given in table 1.

### 2.4. High temperature heat capacity

A Setaram Multi-HTC calorimeter with DSC detector was used to measure the heat capacity of $NaLaF_4$ from 623 K to 1213 K. Temperature calibration was performed with metals (Sn, Zn, Al, Ag, and Au) in aluminum oxide crucibles. The metals were tested at three different heating rates: (1, 2, and 5) $K \cdot min^{-1}$, which provided well-defined, weakly concave parabolic functions. It appeared that the smallest deviations (±1%) from the literature values were obtained with the lower heating rates. After this, four different salts ($Ag_2SO_4$, CsCl, $BaCO_3$, and LiF) were tested in platinum crucibles at the same heating rates. The data points obtained for a given heating rate did not fit in a neat curve, but were scattered around the curve for the metals in $Al_2O_3$ with the same heating rate.

TABLE 1
Measurement series adiabatic calorimetry

| Measurement | Temperature range (K) |
|---|---|
| 1 | 298 to 394 |
| 2 | 94 to 214 |
| 3 | 6 to 30 |
| 4 | 5 to 25 |
| 5 | 28 to 100 |
| 6 | 103 to 300 |
| 7 | 277 to 399 |

A platinum crucible, provided with a boron nitride liner (grade AX05) and a cover, was filled in a dry and pure argon atmosphere with the powdered sample. Then it was quickly transported in a closed capsule to the calorimeter where it was loaded immediately together with an identical empty crucible which was used as the reference. All measurements were carried out under a continuous argon (grade 5.0) flow using the $C_p$-by-step method. This is explained in figure 1. The sample was heated stepwise and during every step the response, *i.e.* the peak was recorded. Intervals of 1.5 h to 2 h between the steps were used to let the instrument equilibrate after each temperature increment. After the experiment, the peak areas were integrated and converted to heat capacity values. For each experiment, three different runs were needed: a run with a sample as was described above, a blank run for the background measurement completed by a run with a standard reference material ($\alpha$-$Al_2O_3$) to obtain a function for the sensitivity. All runs were performed with identical temperature programs.

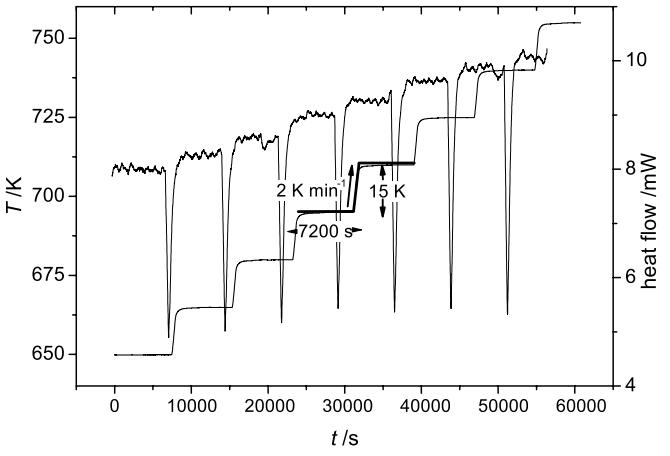


FIGURE 1. Example of a $C_p$-by-step run. The step indicated has a size of 15 K, a rate of $2\ K \cdot min^{-1}$ and a duration of 7200 s.

To process the experimental data, the software package DSCEval [6] was used. The peaks obtained for the sample were corrected for the background signal. Hereafter the signals were converted to $C_{p,m}$ values using the sensitivity function.

To test the new equipment, we first measured pure NaF salt (800 mg) and compared the data to the $C_{p,m}$ function which was derived from the known enthalpy function. After finding a satisfying agreement, we proceeded with $NaLaF_4$ (700 mg). The specific temperature program was the following: from 473 K to 1028 K a step size of 15 K, a heating rate of $2\ K \cdot min^{-1}$ and an isothermal step of 7200 s were selected. From 1018 K to 1078 K a more detailed run was performed with a step size of 5 K, a rate of $2\ K \cdot min^{-1}$ and an isothermal step of 5400 s. In the molten phase from 1053 K to 1213 K the parameters 20 K, $2\ K \cdot min^{-1}$ and 7200 s were chosen.

## 3. The heat capacity of solid NaF

To prove the validity of the high temperature DSC measurements, first $C_{p,m}$ data for NaF were obtained as a test run. Table 2 shows these data for NaF.

A graph is shown in figure 2 containing the high temperature heat capacity data for solid NaF. Added are the low temperature data from King [7] that appears to fit smoothly with the high temperature run. Moreover, the inset graph shows the enthalpy data from O'Brien and Kelley [8] and Macleod [12] plotted as $(H^\circ(T/K) - H^\circ(298.15\ K))/(T - 298.15\ K)$ together with our own data, which were recalculated to the same units for this purpose. It should be noted that the measurement series from Macleod is considered as the more accurate, as it has been suggested that an analytical error exists in the temperature measurements by O'Brien and Kelley [9]. It can be seen that our data, integrated to an enthalpy function mainly overlaps with the data from Macleod. Above 900 K the two series start to diverge, which can probably be ascribed the difference between the direct and indirect (enthalpy) techniques.

The low temperature $C_{p,m}$ data by King and our high temperature $C_{p,m}$ data, combined with the high temperature enthalpy data by Macleod, fit according to the function for $T = 250$ K to $T_{fus}$ (1269 K):

$$C_{p,m}(T/K) = 47.63 + 1.479 \cdot 10^{-2} T/K - 4.643 \cdot 10^{5} (T/K)^{-2}. \quad (1)$$

It can be seen that our $C_{p,m}$ data coincide almost exactly with the combined fit. After the satisfying results on NaF, the similar procedure was applied to $NaLaF_4$.

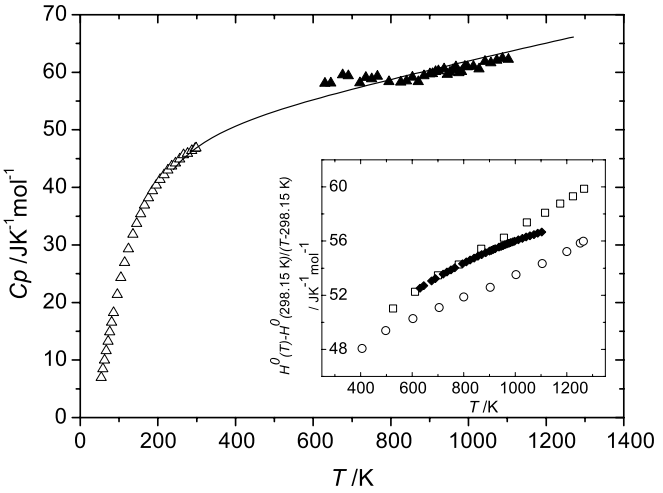


FIGURE 2. Heat capacity data of solid NaF. △: low temperature measurements by King [7]; ▲: our data obtained by heat flow calorimetry; solid line: the combined fit between the low temperature $C_{p,m}$ data [7], our own high temperature $C_{p,m}$ data and the high temperature enthalpy data by Macleod [12]. Inset graph: □: enthalpy data by Macleod [12]; ○: enthalpy data by O'Brien and Kelley [8]; ◆: our data recalculated to enthalpy data.

## 4. The heat capacity of $NaLaF_4$

### 4.1. Heat capacity data at low and high temperature

The data which were obtained by the low temperature adiabatic measurements are presented in table 3. Note that an analytical error exists of ±0.5%, based on the deviation from the used standards [5].

TABLE 2
Heat capacity data of NaF; high temperature measurements

| $T$/K | $C_{p,m}/(J \cdot K^{-1} \cdot mol^{-1})$ | $T$/K | $C_{p,m}/(J \cdot K^{-1} \cdot mol^{-1})$ | $T$/K | $C_{p,m}/(J \cdot K^{-1} \cdot mol^{-1})$ |
|---|---|---|---|---|---|
| 630.6 | 58.08 | 870.6 | 58.37 | 952.5 | 59.98 |
| 645.6 | 58.11 | 885.5 | 59.37 | 967.5 | 60.92 |
| 675.7 | 59.55 | 900.5 | 59.70 | 982.6 | 60.11 |
| 690.6 | 59.36 | 915.5 | 60.11 | 997.5 | 60.91 |
| 720.6 | 58.15 | 945.5 | 59.64 | 1012.6 | 61.02 |
| 735.5 | 59.11 | 960.6 | 60.43 | 1027.6 | 60.56 |
| 750.6 | 58.85 | 975.4 | 59.89 | 1042.6 | 61.86 |
| 765.6 | 59.28 | 990.5 | 61.01 | 1057.7 | 61.63 |
| 795.6 | 58.36 | 907.5 | 59.76 | 1072.7 | 62.08 |
| 825.5 | 58.26 | 922.3 | 60.21 | 1087.8 | 62.41 |
| 840.4 | 58.49 | 937.4 | 60.58 | 1102.9 | 62.25 |
| 855.6 | 59.14 | | | | |

TABLE 3
Heat capacity data of $NaLaF_4$; low temperature measurements

| $T$/K | $C_{p,m}$/(J · K$^{-1}$ · mol$^{-1}$) | $T$/K | $C_{p,m}$/(J · K$^{-1}$ · mol$^{-1}$) | $T$/K | $C_{p,m}$/(J · K$^{-1}$ · mol$^{-1}$) |
|---|---|---|---|---|---|
| | | | *Series 1* | | |
| 298.39 | 139.3 | 332.21 | 143.3 | 363.74 | 145.9 |
| 300.40 | 139.7 | 334.18 | 143.5 | 365.72 | 146.1 |
| 302.41 | 139.9 | 336.15 | 143.4 | 367.70 | 146.3 |
| 304.41 | 140.1 | 338.12 | 143.7 | 369.68 | 145.7 |
| 306.41 | 140.5 | 340.09 | 143.8 | 371.67 | 146.1 |
| 308.40 | 140.8 | 342.06 | 144.0 | 373.65 | 146.5 |
| 310.40 | 141.0 | 344.03 | 144.1 | 375.64 | 146.4 |
| 312.39 | 141.3 | 346.00 | 144.2 | 377.63 | 146.2 |
| 314.38 | 141.7 | 347.97 | 144.4 | 379.63 | 145.9 |
| 316.37 | 141.9 | 349.94 | 144.4 | 381.63 | 146.3 |
| 318.35 | 141.8 | 351.91 | 144.6 | 383.64 | 146.3 |
| 320.34 | 142.0 | 353.88 | 145.1 | 385.65 | 146.2 |
| 322.32 | 142.4 | 355.86 | 144.7 | 387.67 | 146.5 |
| 324.30 | 142.6 | 357.83 | 145.0 | 389.69 | 146.4 |
| 326.28 | 142.8 | 359.80 | 145.3 | 391.71 | 146.8 |
| 328.26 | 143.2 | 361.77 | 145.7 | 393.74 | 146.8 |
| 330.23 | 143.4 | | | | |
| | | | *Series 2* | | |
| 93.73 | 66.87 | 134.65 | 95.17 | 176.27 | 113.8 |
| 95.64 | 68.81 | 136.63 | 96.16 | 178.26 | 114.5 |
| 97.56 | 70.37 | 138.60 | 97.17 | 180.25 | 115.1 |
| 99.48 | 71.80 | 140.57 | 98.34 | 182.24 | 115.9 |
| 101.41 | 73.33 | 142.55 | 99.41 | 184.23 | 116.4 |
| 103.34 | 74.87 | 144.53 | 100.4 | 186.22 | 117.2 |
| 105.28 | 76.29 | 146.51 | 101.3 | 188.21 | 117.8 |
| 107.22 | 77.82 | 148.49 | 102.2 | 190.20 | 118.3 |
| 109.16 | 79.27 | 150.47 | 103.2 | 192.19 | 119.0 |
| 111.11 | 80.67 | 152.45 | 104.1 | 194.18 | 119.5 |
| 113.06 | 81.87 | 154.43 | 105.0 | 196.17 | 120.3 |
| 115.01 | 83.19 | 156.41 | 105.9 | 198.16 | 120.8 |
| 116.96 | 84.63 | 158.40 | 106.7 | 200.16 | 121.2 |
| 118.92 | 85.72 | 160.38 | 107.5 | 202.15 | 122.1 |
| 120.88 | 86.98 | 162.37 | 108.3 | 204.14 | 122.3 |
| 122.84 | 88.13 | 164.35 | 109.3 | 206.14 | 123.0 |
| 124.81 | 89.42 | 166.34 | 109.8 | 208.13 | 123.4 |
| 126.77 | 90.74 | 168.32 | 110.7 | 210.12 | 123.8 |
| 128.74 | 91.87 | 170.31 | 111.7 | 212.12 | 124.4 |
| 130.71 | 92.93 | 172.30 | 112.3 | 214.11 | 124.8 |
| 132.68 | 94.07 | 174.28 | 113.1 | | |
| | | | *Series 3* | | |
| 6.44 | 0.112 | 15.45 | 1.81 | 22.86 | 4.77 |
| 8.52 | 0.362 | 16.67 | 1.90 | 24.16 | 5.55 |
| 10.73 | 0.544 | 17.92 | 2.36 | 25.49 | 6.58 |
| 12.06 | 0.846 | 19.17 | 2.88 | 26.84 | 7.25 |
| 13.14 | 0.952 | 20.38 | 3.40 | 28.23 | 7.62 |
| 14.27 | 1.28 | 21.59 | 4.17 | 29.66 | 8.41 |
| | | | *Series 4* | | |
| 5.00 | 0.31 | 13.72 | 0.94 | 19.66 | 3.22 |
| 6.42 | 0.83 | 14.81 | 1.48 | 20.95 | 3.76 |
| 8.63 | 0.44 | 15.92 | 1.74 | 22.28 | 4.45 |
| 10.43 | 0.63 | 17.13 | 2.14 | 23.61 | 5.23 |
| 11.58 | 0.67 | 18.39 | 2.71 | 24.95 | 6.14 |
| 12.67 | 0.87 | | | | |
| | | | *Series 5* | | |
| 28.19 | 7.48 | 51.56 | 27.55 | 77.40 | 52.31 |
| 29.84 | 8.56 | 53.34 | 29.38 | 79.30 | 54.21 |
| 31.40 | 10.05 | 55.13 | 31.25 | 81.20 | 55.95 |
| 32.95 | 11.54 | 56.93 | 32.91 | 83.11 | 57.83 |
| 34.53 | 12.99 | 58.75 | 34.70 | 85.03 | 59.60 |

(*continued on next page*)

TABLE 3 (*continued*)

| $T$/K | $C_{p,m}/(J \cdot K^{-1} \cdot mol^{-1})$ | $T$/K | $C_{p,m}/(J \cdot K^{-1} \cdot mol^{-1})$ | $T$/K | $C_{p,m}/(J \cdot K^{-1} \cdot mol^{-1})$ |
|---|---|---|---|---|---|
| 36.15 | 14.27 | 60.58 | 36.48 | 86.95 | 61.39 |
| 37.80 | 14.95 | 62.41 | 38.08 | 88.87 | 63.08 |
| 39.47 | 16.26 | 64.26 | 39.83 | 90.80 | 64.71 |
| 41.16 | 17.66 | 66.12 | 41.61 | 92.73 | 66.41 |
| 42.85 | 19.23 | 67.98 | 43.34 | 94.67 | 68.04 |
| 44.57 | 20.85 | 69.85 | 45.17 | 96.61 | 69.53 |
| 46.29 | 22.55 | 71.73 | 46.86 | 98.55 | 71.12 |
| 48.03 | 24.28 | 73.61 | 48.75 | 100.49 | 72.69 |
| 49.79 | 25.92 | 75.50 | 50.53 | | |
| | | | *Series 6* | | |
| 103.07 | 74.58 | 169.24 | 111.3 | 236.05 | 129.9 |
| 105.50 | 76.40 | 171.74 | 112.0 | 238.52 | 130.5 |
| 107.91 | 78.35 | 174.21 | 113.0 | 240.99 | 131.0 |
| 110.33 | 79.90 | 176.68 | 113.8 | 243.45 | 131.6 |
| 112.75 | 81.61 | 179.16 | 114.7 | 245.93 | 132.1 |
| 115.18 | 83.23 | 181.64 | 115.4 | 248.40 | 132.6 |
| 117.60 | 84.89 | 184.12 | 116.4 | 250.88 | 133.1 |
| 120.04 | 86.46 | 186.60 | 117.2 | 253.35 | 133.0 |
| 122.47 | 87.95 | 189.08 | 118.0 | 255.83 | 132.6 |
| 124.91 | 90.18 | 191.57 | 118.7 | 258.31 | 133.1 |
| 127.36 | 91.05 | 194.05 | 119.5 | 260.78 | 133.6 |
| 129.80 | 92.39 | 196.53 | 120.2 | 263.26 | 134.1 |
| 132.25 | 93.77 | 199.00 | 121.0 | 265.73 | 134.5 |
| 134.70 | 95.17 | 201.47 | 121.8 | 268.21 | 135.0 |
| 137.16 | 96.41 | 203.94 | 122.6 | 270.68 | 135.4 |
| 139.61 | 97.75 | 206.41 | 123.0 | 273.15 | 135.8 |
| 142.07 | 98.89 | 208.88 | 123.6 | 275.62 | 136.2 |
| 144.53 | 100.3 | 211.35 | 124.1 | 278.10 | 136.7 |
| 146.99 | 101.5 | 213.82 | 124.7 | 280.57 | 137.1 |
| 149.45 | 102.7 | 216.29 | 125.2 | 283.05 | 137.6 |
| 151.92 | 103.7 | 218.76 | 125.9 | 285.53 | 137.9 |
| 154.39 | 105.0 | 221.23 | 126.3 | 288.01 | 138.3 |
| 156.86 | 106.0 | 223.70 | 127.0 | 290.49 | 138.8 |
| 159.33 | 107.1 | 226.17 | 127.5 | 292.97 | 139.1 |
| 161.80 | 108.1 | 228.64 | 128.1 | 295.45 | 139.2 |
| 164.27 | 109.2 | 231.11 | 128.7 | 297.94 | 139.1 |
| 166.74 | 110.6 | 233.58 | 129.4 | 300.43 | 139.2 |
| | | | *Series 7* | | |
| 276.77 | 136.0 | 318.91 | 140.9 | 361.26 | 144.1 |
| 279.26 | 136.6 | 321.39 | 141.0 | 363.76 | 144.3 |
| 281.74 | 136.5 | 323.87 | 141.4 | 366.27 | 144.3 |
| 284.22 | 137.2 | 326.36 | 141.5 | 368.78 | 144.3 |
| 286.70 | 137.6 | 328.85 | 141.8 | 371.28 | 144.3 |
| 289.17 | 138.2 | 331.34 | 141.9 | 373.79 | 144.8 |
| 291.65 | 138.6 | 333.82 | 142.0 | 376.30 | 145.0 |
| 294.13 | 138.8 | 336.31 | 142.3 | 378.81 | 144.4 |
| 296.60 | 138.8 | 338.80 | 142.6 | 381.33 | 144.8 |
| 299.08 | 139.1 | 341.29 | 142.7 | 383.84 | 145.1 |
| 301.56 | 139.2 | 343.78 | 142.8 | 386.36 | 145.0 |
| 304.03 | 139.7 | 346.28 | 143.1 | 388.88 | 145.2 |
| 306.50 | 140.1 | 348.77 | 143.2 | 391.41 | 145.1 |
| 308.98 | 140.2 | 351.27 | 143.2 | 393.94 | 145.2 |
| 311.46 | 140.3 | 353.76 | 143.3 | 396.47 | 145.3 |
| 313.94 | 140.5 | 356.26 | 143.5 | 398.99 | 145.4 |
| 316.42 | 140.8 | 358.76 | 143.6 | | |

The data obtained by the high temperature heat flux calorimetric measurements on $NaLaF_4$ are presented in table 4.

Data from the low temperature series 3 and 4 were plotted against $T^3$ to find a linear relationship. The value of this parameter was used to calculate the initial values for the integration from 10 K for $H_m$ and $S^\circ_m$. The data were fitted according to the function:

$$C_{p,m}/(J \cdot K^{-1} \cdot mol^{-1}) = 4.23 \cdot 10^{-4}(T/K)^3. \quad (2)$$

TABLE 4
Heat capacity data of $NaLaF_4$; high temperature measurements

| $T$/K | $C_{p,m}/(J \cdot K^{-1} \cdot mol^{-1})$ | $T$/K | $C_{p,m}/(J \cdot K^{-1} \cdot mol^{-1})$ | $T$/K | $C_{p,m}/(J \cdot K^{-1} \cdot mol^{-1})$ |
|---|---|---|---|---|---|
| 630.5 | 169.4 | 765.5 | 173.7 | 900.4 | 184.1 |
| 645.7 | 178.6 | 780.6 | 180.1 | 915.4 | 185.9 |
| 660.5 | 169.7 | 795.6 | 177.3 | 930.5 | 190.6 |
| 675.7 | 173.4 | 810.5 | 178.3 | 945.5 | 190.1 |
| 690.6 | 167.0 | 825.5 | 182.4 | 960.5 | 190.9 |
| 705.5 | 169.1 | 840.5 | 182.8 | 975.5 | 189.3 |
| 720.5 | 172.6 | 855.5 | 180.6 | 990.5 | 198.8 |
| 735.6 | 170.7 | 870.5 | 192.4 | 1005.5 | 197.2 |
| 750.4 | 169.2 | 885.5 | 181.7 | 1020.4 | 211.5 |
| | | | *Detailed* | | |
| 1020.5 | 311.0 | 1035.5 | 310.0 | 1060.5 | 2159.3 |
| 1025.5 | 312.7 | 1040.5 | 325.4 | 1065.5 | 412.0 |
| 1020.5 | 311.4 | 1045.6 | 389.5 | 1070.5 | 318.7 |
| 1025.5 | 312.5 | 1050.7 | 625.7 | 1075.5 | 306.7 |
| 1030.5 | 318.2 | 1055.6 | 1261.8 | | |

TABLE 5
Heat capacity and entropy of $NaLaF_4$ at selected temperatures from 10 K to 1200 K

| $T$/K | $C^{\circ}_{p,m}/(J \cdot K^{-1} \cdot mol^{-1})$ | $S^{\circ}_{m}(T)/(J \cdot K^{-1} \cdot mol^{-1})$ | $T$/K | $C^{\circ}_{p,m}/(J \cdot K^{-1} \cdot mol^{-1})$ | $S^{\circ}_{m}(T)/(J \cdot K^{-1} \cdot mol^{-1})$ |
|---|---|---|---|---|---|
| 10 | 0.655 | 0.141 | 120 | 86.4 | 59.1 |
| 15 | 1.58 | 0.479 | 130 | 92.5 | 66.3 |
| 20 | 3.29 | 1.14 | 140 | 97.9 | 73.3 |
| 25 | 6.18 | 2.16 | 150 | 102.9 | 80.3 |
| 30 | 8.72 | 3.50 | 160 | 107.3 | 87.0 |
| 35 | 13.4 | 5.20 | 170 | 111.5 | 93.6 |
| 40 | 16.7 | 7.19 | 180 | 115.0 | 100.1 |
| 45 | 21.3 | 9.41 | 190 | 118.3 | 106.4 |
| 50 | 26.1 | 11.9 | 200 | 121.3 | 112.5 |
| 55 | 31.1 | 14.6 | 210 | 123.8 | 118.5 |
| 60 | 35.9 | 17.5 | 220 | 126.1 | 124.3 |
| 65 | 40.5 | 20.6 | 230 | 128.5 | 130.0 |
| 70 | 45.3 | 23.8 | 240 | 130.8 | 135.5 |
| 75 | 50.1 | 27.1 | 250 | 132.9 | 140.9 |
| 80 | 54.9 | 30.4 | 260 | 133.4 | 146.1 |
| 85 | 59.6 | 33.9 | 270 | 135.3 | 151.2 |
| 90 | 64.0 | 37.4 | 280 | 136.9 | 156.1 |
| 95 | 68.3 | 41.0 | 290 | 138.6 | 160.9 |
| 100 | 72.3 | 44.6 | 298.15 | 139.1 | 164.8 |
| 105 | 76.0 | 48.2 | 300 | 139.7 | 165.7 |
| 110 | 79.7 | 51.9 | 310 | 140.2 | 170.2 |
| 320 | 141.0 | 174.7 | 725 | 170.9 | 300.4 |
| 330 | 141.9 | 179.0 | 750 | 172.9 | 306.2 |
| 340 | 142.7 | 183.3 | 775 | 175.0 | 311.9 |
| 350 | 143.2 | 187.4 | 800 | 177.1 | 317.5 |
| 360 | 143.8 | 191.5 | 825 | 179.3 | 323.0 |
| 370 | 144.3 | 195.4 | 850 | 181.5 | 328.4 |
| 380 | 144.6 | 199.3 | 875 | 183.8 | 333.7 |
| 390 | 145.1 | 203.0 | 900 | 186.0 | 338.9 |
| 400 | 146.8 | 206.8 | 925 | 188.4 | 344.0 |
| 425 | 148.6 | 215.7 | 950 | 190.7 | 349.1 |
| 450 | 150.4 | 224.3 | 975 | 193.1 | 354.0 |
| 475 | 152.1 | 232.5 | 1000 | 195.6 | 359.0 |
| 500 | 153.9 | 240.3 | 1025 | 198.1 | 363.8 |
| 525 | 155.7 | 247.9 | 1050 | 200.6 | 368.6 |
| 550 | 157.5 | 255.1 | 1075 | 203.2 | 373.4 |
| 575 | 159.3 | 262.2 | 1100 | 205.8 | 378.1 |
| 600 | 161.1 | 269.0 | 1125 | 208.4 | 382.7 |
| 625 | 163.0 | 275.6 | 1150 | 211.1 | 387.3 |
| 650 | 164.9 | 282.1 | 1175 | 213.9 | 391.9 |
| 675 | 166.9 | 288.3 | 1200 | 216.7 | 396.4 |
| 700 | 168.9 | 294.4 | | | |

This equation results in $S^{\circ}_{m}(10\ \mathrm{K}) = 0.141\ \mathrm{J \cdot K^{-1} \cdot mol^{-1}}$ and $H_{m}(10\ \mathrm{K}) = 1.0575\ \mathrm{J \cdot mol^{-1}}$. The heat capacity and entropy values were determined by numerical integration followed by interpolation of the values of the experimental data points. The results can be found in table 5. Added are the values that were derived from the high temperature measurements. The values between 400 K and 600 K are obtained by interpolation between the low and the high temperature series.

The following values at $T = 298.15$ K were extracted from table 5:

$$C_{p,m}(298.15\ \mathrm{K}) = 139.1\ \mathrm{J \cdot K^{-1} \cdot mol^{-1}}, \quad (3)$$

$$S^{\circ}_{m}(298.15\ \mathrm{K}) = 164.8\ \mathrm{J \cdot K^{-1} \cdot mol^{-1}}, \quad (4)$$

$$H^{\circ}_{m}(298.15\ \mathrm{K}) - H^{\circ}_{m}(0\ \mathrm{K}) = 25,901\ \mathrm{J \cdot mol^{-1}}. \quad (5)$$

After processing the data of the heat flow calorimetric measurements, both series, for the low and the high temperature, were plotted in figure 3, with a more detailed plot of the data excluding the prominent peak in figure 4.

The function that fits the $C_{p,m}$ function for $298.15 < T/\mathrm{K} \leqslant 1010$ K, with an average error of 0.75%, is:

$$C_{p,m}(T/\mathrm{K}) = 132.61 + 2.9109 \cdot 10^{-2} T/\mathrm{K} + 3.4332 \cdot 10^{-5} (T/\mathrm{K})^2 - 4.6607 \cdot 10^{5} (T/\mathrm{K})^{-2}. \quad (6)$$

The peak at 1060 K is interpreted as the decomposition of $NaLaF_4$, since it is known as an incongruently melting compound [1,10], giving rise to the peritectic in the binary system ($NaF + LaF_3$). Above this temperature, the compound is decomposed in solid $LaF_3$ plus a liquid, persisting in equilibrium up to 1400 K, where the liquidus is crossed [2]. The data from 1060 K to 1213 K in figure 3 cannot therefore be interpreted as the $C_{p,m}$ of liquid $NaLaF_4$.

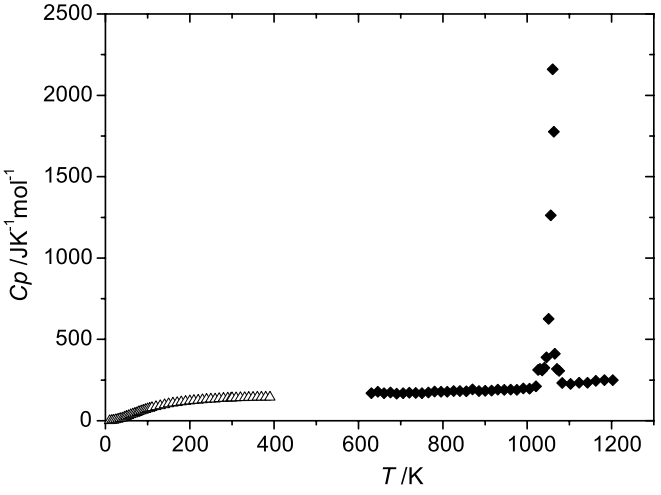


FIGURE 3. Heat capacity measurements on $NaLaF_4$. △: obtained by adiabatic calorimetry; ◆: obtained by heat flow calorimetry.

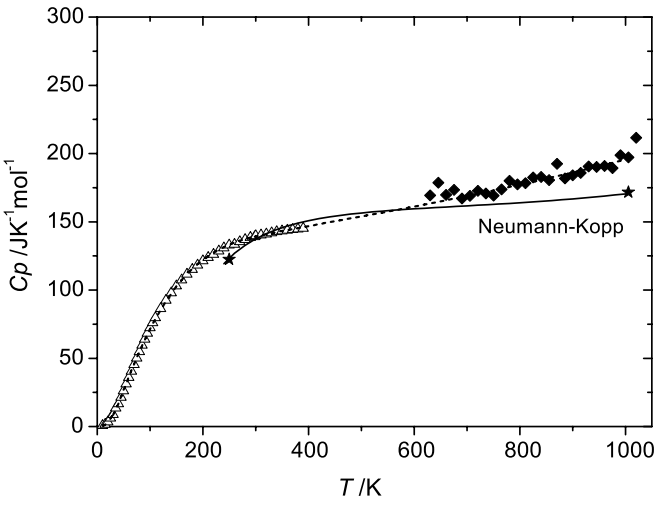


FIGURE 4. Detailed image of the heat capacity data of $NaLaF_4$ together with the fitting function till 1000 K plotted.

### 4.2. Comparison with the Neumann–Kopp rule

Figure 4 also shows the empirical $C_{p,m}$ of $NaLaF_4$ according to the Neumann–Kopp rule. The $C_{p,m}$ functions of NaF and $LaF_3$, which were used in a previous paper [2] to assess ($LiF + NaF + LaF_3$), are added here. It can be seen that this rule is only valid in the temperature range between 300 K and 700 K. At higher temperatures the Neumann–Kopp rule considerably underestimates the observed $C_{p,m}$ data, probably because the lattice interactions in the compound are significantly different compared to those in the pure components, leading to different anharmonic contributions to the heat capacity.

### 4.3. Reassessment of the ($NaF + LaF_3$) phase diagram

The ($NaF + LaF_3$) diagram was reassessed using the obtained $C_{p,m}$ data on $NaLaF_4$. The thermodynamic assessment is briefly described here; more details can be found in van der Meer *et al.* [2].

The Gibbs free energy functions for the relevant compounds were needed in the model and were set up after careful investigation of thermodynamic tables [11]. The function is described by equation (7) as the contribution of the enthalpy of formation and the absolute entropy at the reference state plus a contribution of the heat capacity $C_{p,m}$ as a polynomial function of $T$:

$$G(T) = \Delta_f H^{\circ}_{m}(298.15\ \mathrm{K}) - S^{\circ}_{m}(298.15\ \mathrm{K})T + \sum a_i T^i. \quad (7)$$

General polynomials were used to describe the excess Gibbs free energy coefficients that define the shape of a phase diagram. The equation for a binary system (A + B) is given in the following equation:

$$\Delta_{xs} G = L^{p,q}_{A,B}(T) Y_A \left(\frac{\chi_i}{\chi_i + \chi_j}\right)^{p} Y_B \left(\frac{\chi_j}{\chi_i + \chi_j}\right)^{q}, \quad (8)$$

where $L^{p,q}_{A,B}(T)$ is the excess Gibbs free energy term as a function of the temperature. $Y_A$ and $Y_B$ are the equivalent

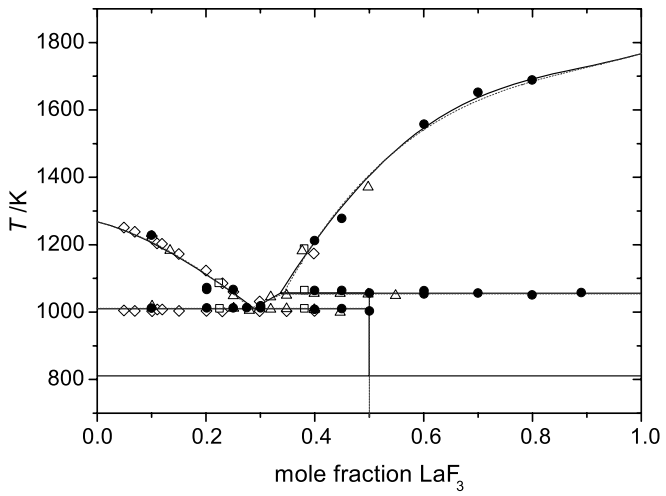


FIGURE 5. The ($NaF + LaF_3$) diagram reassessed with the $C_{p,m}$ data for $NaLaF_4$. Solid line: with $C_{p,m}$ data obtained by this study; dashed line: with optimized $C_{p,m}$ data, taken from our previous study [2]. ●: our own experimental data [2]; △: Abdoun *et al.* [1]; ◇: Matthes and Holz [13]; □: Grande [14], the last two as a reference in [1].

fractions of the components, while $\chi_i$ and $\chi_j$ are the sum of the equivalent fractions in the same symmetry group with $i$ and $j$ as indices for the group numbers. It should be noted that it is possible to rewrite the well-known Redlich–Kister equation for binary interactions in the general polynomial notation in this case, as the equivalent fractions are similar to the mole fractions.

The excess Gibbs free energy terms for the solution phase were optimized together with $\Delta_f H^\circ_m(298.15\ K)$ of $NaLaF_4$, which is still an unknown. This resulted in an excellent fit with the experimental data, but the compound is only stable above 810 K. This result is shown in figure 5, where it is compared to the old diagram, which was calculated by optimizing the complete Gibbs free energy function of $NaLaF_4$ [2]. The standard enthalpy of formation, the standard entropy and the heat capacity functions that were used are found in table 6. The optimized excess Gibbs free energy coefficients, for the old and the new assessment are listed in table 7.

In an attempt to have the compound stable at room temperature, the $\Delta_f H^\circ_m(298.15\ K)$ was fixed in the assessment and only the excess Gibbs terms were optimized. This resulted in a diagram where the liquidus at the $LaF_3$ side became a plateau and the value of the eutectic point shifted to a temperature too low and a NaF content too high than could be justified by the experimental data. Preferred was then the diagram that gives a correct description of the liquidus and the eutectic and peritectic points, since the final goal of this study is a better understanding of the phase behavior of molten fluorides for Molten Salt Reactor applications. The introduction of additional $T\ln T$ and/or $T^2$ terms in the equation used to describe the temperature dependence of the excess Gibbs free energy of the liquid did not improve the fit.

TABLE 7
Optimized excess Gibbs parameters of the liquid phase for ($NaF + LaF_3$) by the polynomial model

| (A + B) | $p$ | $q$ | ${}^0L_{A,B}/(J\cdot mol^{-1})$ | ${}^1L_{A,B}/(J\cdot K^{-1}\cdot mol^{-1})$ |
|---|---|---|---|---|
| ($NaF + LaF_{3,old}$) | 0 | 0 | −67,708 | 128.27 |
| | 1 | 0 | −10,990 | 14.895 |
| | 0 | 1 | 9563.4 | −13.882 |
| ($NaF + LaF_{3,reass}$) | 0 | 0 | −41,675 | 17.693 |
| | 1 | 0 | −31,473 | 21.301 |
| | 0 | 1 | 10,122 | −27.354 |

The difference between the old and the new, experimentally based diagram can be explained by the relatively large difference in the standard entropy of formation. In the old assessment, a value of $S^\circ_m(298.15\ K) = 155.5\ J\cdot K^{-1}\cdot mol^{-1}$ resulted from the optimization, while the measured value is $164.8\ J\cdot K^{-1}\cdot mol^{-1}$, as came out in this study.

The difference between on the one hand the sum of $\Delta_f G^\circ_m(298.15\ K)$ for NaF and $LaF_3$ and on the other hand $\Delta_f G^\circ_m(298.15\ K)$ for $NaLaF_4$, which was calculated using the experimental $S^\circ_m(298.15\ K)$ and the optimized $\Delta_f H^\circ_m(298.15\ K)$, was $+4053\ J\cdot mol^{-1}$. This indicates that, according to the thermodynamic model, the compound is not stable at room temperature. But this positive value is only small and it is explainable that a small discrepancy exists between the model and the experiments. It should be noted that this is an uncertainty of 0.18% compared to the optimized $\Delta_f H^\circ_m(298.15\ K)$ of $2240\ kJ\cdot mol^{-1}$, which is smaller than the analytical error in the low temperature heat capacity

TABLE 6
$\Delta_f H^\circ_m(298.15\ K)$, $S^\circ_m(298.15\ K)$, and $C_{p,m}$ data for the NaF, $LaF_3$, and $NaLaF_4$

| Compound | $\Delta_f H^\circ_m(298.15\ K)/(kJ\cdot mol^{-1})$ | $S^\circ_m(298.15\ K)/(J\cdot K^{-1}\cdot mol^{-1})$ | [a] | $T/K^b$ | $T^2/K^{2c}$ | $T^{-2}/K^{-2d}$ |
|---|---|---|---|---|---|---|
| NaF(l)[a] | −558.583 | 50.778 | 72.989 | | | |
| $LaF_3$(l)[a] | −1633.920 | 97.639 | 135.00 | | | |
| NaF(cr)[a] | −576.650 | 51.210 | 42.554 | 1.9881E − 02 | | −3.8773E + 05 |
| $LaF_3$(cr)[a,b] | −1669.500 | 106.980 | 122.119 | −2.2467E − 02 | −1.6309E − 05 | −2.1714E + 06 |
| $NaF\cdot LaF_3$(cr)[c] | −2254.924 | 155.515 | 165.00 | −5.4388E − 03 | −1.6309E − 05 | −2.2682E + 06 |
| $NaF\cdot LaF_3$(cr)[d] | −2240.125 | 164.800 | 132.61 | 2.9109E − 02 | 3.4332E − 05 | −4.6607E + 05 |

[a] Data taken from an internal report [15].
[b] A small, but significant extra term appears in the $C_{p,m}$ function: $2.8175E-08T^3$.
[c] Obtained by assessment with polynomial model.
[d] Obtained by $C_{p,m}$ measurements; $\Delta_f H^\circ(298.15\ K)$ is optimized.

measurements (0.5%) and the error in the fit of the $C_{p,m}$ function (0.75%).

## 5. Conclusion

The heat capacity of solid NaF was measured using differential scanning heat flux calorimetry. The results showed a good agreement with the low temperature data by King [7] on the one hand and with the high temperature data by Macleod [12] on the other hand.

The similar technique was applied on $NaLaF_4$, which was synthesized *in situ* from NaF and $LaF_3$ in the calorimeter and its purity was checked by XRD analysis. In addition to the high temperature heat capacity measurements, adiabatic calorimetry was used to perform low temperature measurements, from 4 K to 400 K, as well. The two data series fitted smoothly.

A comparison with the Neumann–Kopp rule showed that the sum of the $C_{p,m}$ of NaF and $LaF_3$ describes the experimental curve well up to about 700 K. Above this temperature the empirical $C_{p,m}$ values are smaller than the experimental values, probably due to the fact that the lattice interactions in the compound start to differ significantly from those in the pure components.

The newly obtained standard entropy of formation and the $C_{p,m}$ function for $NaLaF_4$ were used in a reassessment of the system ($NaF + LaF_3$). The agreement with the experimental data was good, although the compound was stable only above 810 K. This could be explained by the small discrepancy between model and experiments, which falls in the error range of the heat capacity measurements and the mathematical fit of the $NaLaF_4$ $C_{p,m}$ function.

## Acknowledgement

The authors thank Daniel Bouëxierre from ITU for his XRD analysis.

## References

[1] F. Abdoun, M. Gaune-Escard, G. Hatem, J. Phase Equilibr. 18 (1997) 6.
[2] J.P.M. van der Meer, R.J.M. Konings, K. Hack, H.A.J. Oonk, Chem. Mater. 16 (2006) 510.
[3] W.H. Zachariasen, Acta Crystallogr. 1 (1948) 265.
[4] J.H. Burns, Inorg. Chem. 4 (1965) 881.
[5] J.C. van Miltenburg, G.J.K. van den Berg, M.J. van Bommel, J. Chem. Thermodyn. 19 (1987) 1129.
[6] D. Sedmidubský, O. Beneš, R.J.M. Konings, J. Chem. Thermodyn. 37 (2005) 1098.
[7] E.G. King, J. Am. Ceram. Soc. 79 (1957) 2056.
[8] C.J. O'Brien, K.K. Kelley, J. Am. Ceram. Soc. 79 (1957) 5616.
[9] W.B. Frank, J. Phys. Chem. 65 (1961) 2081.
[10] R.E. Thoma, H. Insley, G.M. Hebert, Inorg. Chem. 5 (1966) 1937.
[11] M.W. Chase Jr. (Ed.), NIST-JANAF Thermochemical Tables Fourth Edition, J. Phys. Chem. Ref. Data Monograph 9.
[12] A.C. Macleod, J. Chem. Soc., Faraday Trans. I 69 (1973) 2026.
[13] F. Matthes, S. Holz, Z. Chem. 2 (1962) 22.
[14] T. Grande, Ph.D. Thesis, University of Trondheim, 1992.
[15] R.J.M. Konings, J.P.M. van der Meer, E. Walle, Chemical aspects of Molten Salt Reactor Fuel, European Commission Joint Research Centre, 2005, JRC-ITU-TN 2005/25.

JCT 05-308